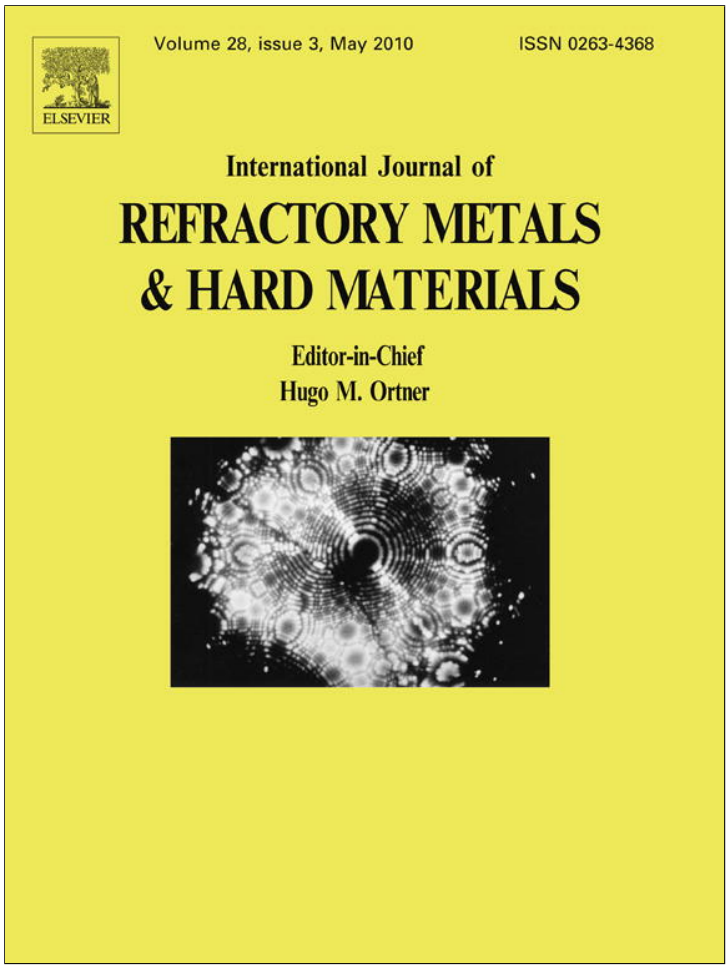

Int. Journal of Refractory Metals & Hard Materials 28 (2010) 446–450

Contents lists available at ScienceDirect

Int. Journal of Refractory Metals & Hard Materials

journal homepage: www.elsevier.com/locate/IJRMHM

Small tungsten carbide nanoparticles: Simulation of structure, energetics, and tensile strength

V.G. Zavodinsky *

Institute for Materials Science of the Russian Academy of Sciences, 153 Tikhookeanskaya Str., Khabarovsk 680042, Russian Federation

ARTICLE INFO

Article history:
Received 27 December 2009
Accepted 8 February 2010

Keywords:
Tungsten carbide
Nanoparticles
Ab initio calculations
Tensile strength

ABSTRACT

Ab initio methods of the density functional theory and pseudopotentials were used to study the structure, electronic states, total energy and tensile strength of WC nanoparticles. It has been found that the very small particles (having less than 15 WC atomic pairs) have a cube-like NaCl structure. Particles with trigonal and cubic structures have approximately the same energies in the region of 10–20 WC pairs; however, the local atomic structure keeps the NaCl-like alternation of W and C atoms. The WC_{15} trigonal particle was used as a typical one to study the WC nanoparticle tensile strength. It has been found that W and C vacancies decrease the tensile strength, but not drastically. Electronic structure of nanoparticles looks like that of bulk *fcc*-WC with a large density of states at the Fermi level.

1. Introduction

The hard alloys based on tungsten carbide are widely used as a material for cutting tools. Recent investigations show that the work characteristics of hard alloys improve very much due to decreasing of the crystallite sizes to 300–500 nm [1–4]. However, the origin of such drastic changes is not known. Furthermore, it is not clear how the properties of the hard alloys will be changed due to decreasing of WC crystallites to the nanometer scale. Besides, there is a lack of information on the atomic and electronic structures and mechanical properties of WC nanoparticles. It is reported [5,6] that the 300–500 nm particles have a trigonal shape; however, their internal structure is unknown. Especially, there is no information on structure and properties of particles with the sizes in 100 nm and smaller.

This work is devoted to the *ab initio* quantum–mechanical simulation of the small tungsten carbide nanoparticles (equal or less than 1 nm in size) and to study their electronic structure and mechanical properties. Certainly, one nanometer is too small a size to predict correctly the properties of particles in the size of 50–100 nm which are of interest for technology. As it is very difficult to study larger particles with *ab initio* methods so I believe that my investigation of small particles will be a useful attempt to say something about this 'terra incognita'.

2. Methods and approaches

The total energies, electronic structures and mechanical properties of WC nanoparticles were calculated using the density functional theory (DFT) [7,8], the pseudopotential method [9] and the plane wave basis set for presentation of wave functions.

The DFT is based on consequence of the Hohenberg and Kohn theorem [7] from which it is follows that one-particle electron energies ε_i and wave functions ψ_i may be found from a set of equations

$$\left(-\frac{h^2}{2m}\nabla^2 + V_{\text{eff}}(\boldsymbol{r})\right)\psi_i(\boldsymbol{r}) = \varepsilon_i\psi_{\boldsymbol{i}}(\boldsymbol{r}),$$

where V_{eff} is an effective potential,

$$V_{\text{eff}} = V_{\text{ext}}(\boldsymbol{r}) + \int \frac{e^2 n(\boldsymbol{r}')}{|\boldsymbol{r}-\boldsymbol{r}'|} d^3\boldsymbol{r}' + V_{\text{XC}}(\boldsymbol{r})$$

and V_{XC} is the exchange–correlation potential for which a number of possible approximations may be made. Most popular of the approximations are the local density approximation (LDA) [10,11] and the generalized gradient approximation (GGA) [12]. In cases where the external potential is spin dependent, an approximation must be made to V_{XC}, which depends on both the total electronic density $n(\boldsymbol{r}) = \boldsymbol{n}\uparrow(\boldsymbol{r}) + \boldsymbol{n}\downarrow(\boldsymbol{r})$ and the polarization $\xi(\boldsymbol{r}) = \frac{n\uparrow(\boldsymbol{r})-n\downarrow(\boldsymbol{r})}{n(\boldsymbol{r})}$, where $n\uparrow(\boldsymbol{r})andn\downarrow(\boldsymbol{r})$ are the densities of spin up and spin down electrons, respectively.

If all of the electrons in a system were explicitly included in the calculation, V_{ext} would be constructed from the full Coulombic

* Tel.: +7 4212 226956; fax: +7 4212 226598.
E-mail address: vzavod@mail.ru

0263-4368/$ - see front matter © 2010 Elsevier Ltd. All rights reserved.
doi:10.1016/j.ijrmhm.2010.02.003

potential of the nuclei. The rapid oscillations of the wavefunctions near to the nucleus, due to the very strong potential in the region and the orthogonality condition between different states, mean that a very large basis set would be necessary. Fortunately, the core electrons on different atoms are almost independent of the environment surrounding the atom and that only the valence electrons participate strongly in interactions between atoms. Thus, the core electron states may be assumed to be fixed and a pseudopotential may be constructed for each atomic species which takes into account the effects of the nucleus and core electrons [9]. The pseudowavefunctions corresponding to this modified potential do not exhibit the rapid oscillations of the true wavefunctions, dramatically reducing the number of plane waves needed for their representation. The calculations then need only explicitly consider the valence electrons, offering a further saving in effort.

A pseudopotential is constructed such that it matches the true potential outside a given radius, designated the core radius. Similarly, each pseudowavefunction must match the corresponding true wavefunction beyond this distance. In addition, the charge densities obtained outside the core region must be identical to the true charge density. Thus, the integral of the squared amplitudes of the real and pseudo wave functions over the core region must be identical. This condition is known as norm-conservation [13].

The atomic properties of the element must be preserved, including phase shifts on scattering across the core. These phase shifts will be different for different angular momentum states and so, in general, a pseudopotential must be non-local, with projectors for different angular momentum components. The pseudopotential is often represented using the separable form [14]

$$V = V_{\mathrm{loc}} + \sum_{l,m} (V_l - V_{\mathrm{loc}}) \hat{P}_{l,m},$$

where $\hat{P}_{l,m}$ are the projectors which project the electronic wave functions onto the eigenfunctions of different angular momentum states. The choice of V_{loc} is arbitrary and if it is made equal to one of the V_l this avoids the need for the corresponding set of angular momentum projectors.

Because pure tungsten carbide (without cobalt) is not magnetic material I have used the spin-restricted version of DFT realized within the FHI96md package [15] previously used with advantage for many systems, including transition metal compositions [16–19]. In all cases, the GGA approach to description of the exchange–correlation interactions has been chosen and the optimization of the atomic geometry has been performed. The equilibrium lattice constants and bulk modules were calculated using Murnagham equation of state [20].

In this work, I used the pseudopotentials of carbon constructed with the FHI98PP package [21] in the scheme of Troullier and Martins [22], but for tungsten, I used the scheme of Hamann [13]. Pseudopotentials were constructed using an *ab initio* procedure. The true wavefunctions were calculated for an isolated atom using an all-electron DFT approach. The resulting valence wavefunctions were then modified in the core region to remove the oscillations while obeying the norm-conservation constraint. The Schrödinger equation was then inverted to find the pseudopotential which will reproduce the pseudowavefunctions. This procedure produces pseudopotentials which may be transferred between widely varying systems. All these pseudopotentials are separable, transferable, and norm-conserving ones. They were checked for the absent of the so-called 'ghost' states and used for determining the equilibrium lattice parameters and the bulk elastic modulus of WC. The parameters of pseudopotentials are listed in Table 1.

The FHI96md package operates with periodic wave functions. Thus, to investigate nanoparticles I used cubic 30–40 a.u. supercells (1 a.u. is equal to 0.0529 nm) those were large enough to study nanoparticles up to 1 nm of size as single, noninteracting

Table 1
Critical radii of the *s*, *p*, and *d* components (r_s, r_p, r_d), and types of local parts (l_{loc}) of pseudopotentials.

Element	r_s (Å)	r_p, (Å)	r_d, (Å)	l_{loc}
W	1.57	1.78	0.88	*s*
C	1.50	1.50	1.50	*d*

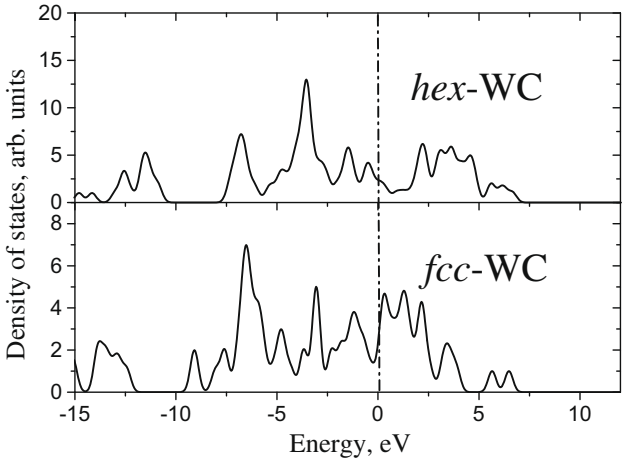

Fig. 1. Calculated densities of states for hexagonal (*hex*-WC) and cubic (*fcc*-WC) tungsten carbide. Vertical dotted line shows the Fermi level.

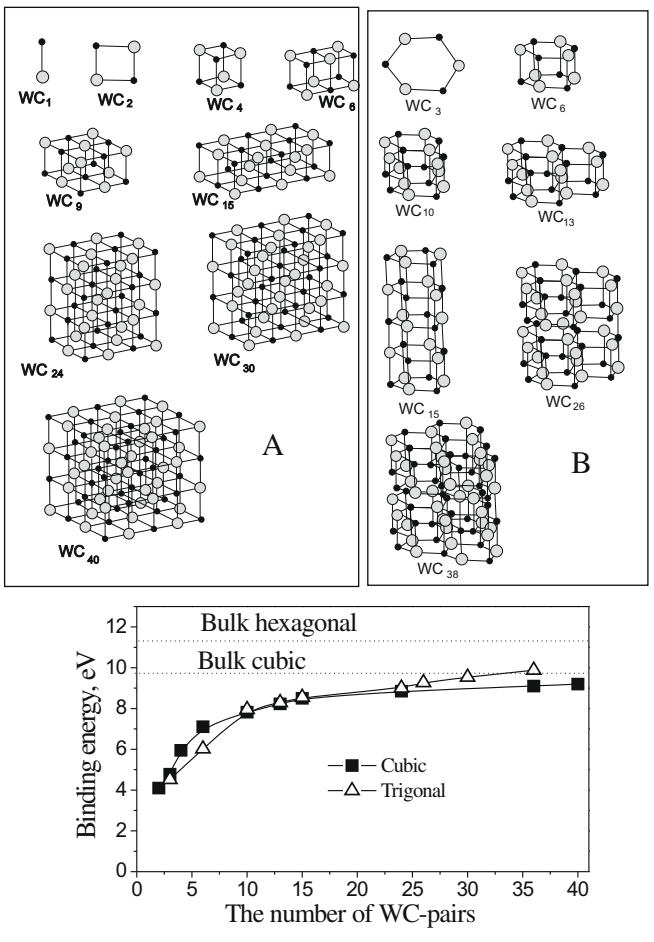

Fig. 2. Atomic schemes of WC nanoparticles with cubic (A) and trigonal (B) structure. Small black circles are C atoms, large gray circles are W atoms. The low panel represents dependence of the binding energy (per WC pair) on the structure and the size of WC nanoparticles.

particles. In the majority of cases (except bulk calculations) I used one point in the Brillouin zone, namely, the Γ-point (0, 0, 0). For bulk calculations, the Monkhorst and Pack schemes [23] ($3 \times 3 \times 3$ and $5 \times 5 \times 5$) were implemented with the number of k-points up to 27. The energy cutoff for the plane wave set was equal to 40 Ry. The self-consistence convergence was provided by stabilizing the total energy with an accuracy of 0.005 eV.

3. Results and discussions

3.1. Bulk calculations

It is assumed that the bulk tungsten carbide structure is well known. The hexagonal WC is stable under 2525 °C and the *fcc* NaCl-like WC structure is stable above this temperature [24].

For *hex*-WC I have found the lattice constant a of 2.92 Å, the cohesive energy E_{coh} of 9.69 eV, and the bulk module B of 388 GPa: experimental values are a = 2.91 Å, E_{coh} = 8.34 eV, and B = 331 GPa [25]. Published theoretical data lay in the intervals of 2.88–2.92 Å, 379–413 GPa, and 8.14–9.72 eV, respectively [26].

For cubic *fcc*-WC I have calculated a = 4.39 Å and E_{coh} = 8.89 eV. Respective published values are 4.29–4.38 Å and 7.71–9.46 eV, respectively [28].

Besides I have calculated the densities of electronic states (DOS) and plotted them in Fig. 1. The DOS for *hex*-WC and *fcc*-WC look very much like the literature data [25,27,28]. The main difference of the *fcc* DOS from the *hex* one consists of different densities of states at the Fermi level. Namely, in the *hex* case the Fermi level is situated close to a minimum while in the *fcc* case its position lies near a maximum.

3.2. Atomic structures and electronic states of nanoparticles

There is experimental and theoretical information [5,6,28–33] that tungsten carbide crystals are trigonal rather than hexagonal. However, it is unknown what the atomic structure of WC nanoparticles, their electronic structure and their properties are.

I have studied stoichiometric particles with the number (N) of WC pairs from 2 up to 40 (with the linear size from 0.2 to 1 nm) and have compared their binding energies per WC pair. First I have found that the NaCl-like bonding is preferable for all studied WC structures. Hexagonal particles with the bulk-like (layer by layer) W and C ordering are not stable: they are transformed spontaneously to triangular ones with the NaCl ordering. Triangular particles compete with the particles having a cubic symmetry: for $N < 15$ the cubic particles are preferable but for $N > 15$ the triangular ones demonstrate the energy gain. Atomic schemes of some studied particles with cubic and trigonal symmetry are shown in Fig. 2A and B and the dependence of the binding energy on the structure and size of particles is plotted in Fig. 2C.

Despite of the W–C bonding in nanoparticles has the same Na–Cl type as in bulk *fcc*-WC, the lengths of W–C bonds in nanoparticles are different from the bulk ones. Namely, in the relaxed WC_{15} trigonal particle the W–C distances are varied from 1.98 to 2.20 Å, in the relaxed WC_{24} cubic particle the corner distances are equal to 1.98 Å, and they increase up to 2.40 Å when going to the center of the particle. At the whole, the average W–C distances ($d(W–C)_{av}$) in trigonal particles are less than in cubic ones (Table 2). Besides, the average W–C distances in trigonal particles stabilize quickly to the 2.04 Å, while in the cubic particles they have a tendency to growth up to the bulk value of 2.20 Å. Perhaps

Table 2
The average W–C distances $d(W–C)_{av}$ in cubic and trigonal WC particles.

(Å)	WC_6		WC_{15}		WC_{24}		WC_{36}	
	Cubic	Trigonal	Cubic	Trigonal	Cubic	Trigonal	Cubic	Trigonal
$d(W–C)_{av}$	2.07	1.98	2.11	2.04	2.12	2.04	2.13	2.04

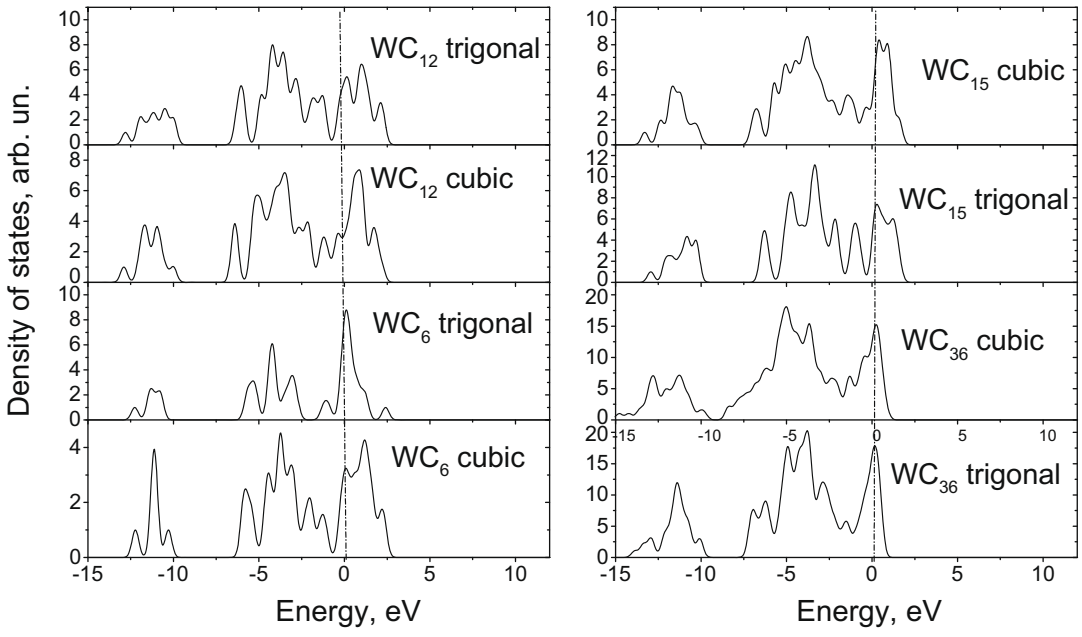

Fig. 3. The densities of states for the WC cubic and trigonal nanoparticles. Vertical dotted lines represent the Fermi level.

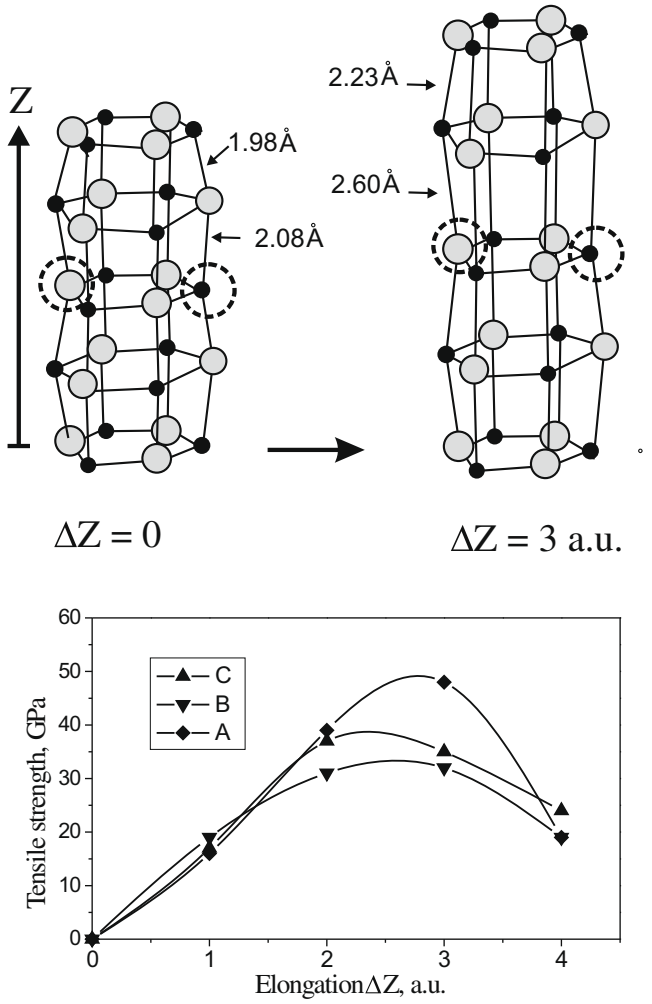

Fig. 4. Tensile strength studying for the WC_{15} trigonal particle. (A) A perfect particle; (B) a particle with a W-vacancy; and (C) a particle with a C-vacancy. Dotted circles show the places for W and C vacancies. The low panel shows the dependence of the tensile strength on the particle elongation ΔZ. A vertical arrow *Z* represents the direction of elongation.

this is a main reason why the trigonal particles become more favorable at large particle sizes.

The electronic structure of WC nanoparticles is presented in Fig. 3. The all plotted densities of states (DOS) look like the DOS of bulk *fcc*-WC shown above in Fig. 1. Namely, they have a metallic character with the position of the Fermi level near a local maximum of the DOS. One can suppose that the origin of such similarity is the similarity of W–C bonding in all our particles (either cubic or trigonal). This bonding is a NaCl-like, and the *fcc*-WC has the same bonding.

3.3. Tensile strength

Tensile strength is one of the most important mechanical properties of tungsten carbide as a material for the cutting tools. Usually three kinds of the tensile strength tests are used: breaking off, bending, and compression. In the case of nanoparticles, the test for breaking off seems the most comprehensible. As trigonal particles are more stable than cubic ones, I have studied tensile strength for the trigonal case, namely, for the WC_{15} particle.

To find the tensile strength I elongated (step by step) the WC_{15} particle along the *Z* axis, keeping the edge atoms and relaxing the rest on the each step (Fig. 4). The value of strength *T* was calculated through a derivation of the total energy *E* as a function of *z*:

$$T = \frac{dE}{dz} \cdot \frac{1}{S},$$

where *S* is an across square of the particle.

The plot of *T* as a function of elongation ΔZ is presented in Fig. 4 (A curve). The maximum point of this plot corresponds to $T = 48$ GPa that is much more than known values for bulk tungsten carbide (0.3–0.4 GPa) and hard alloys on its basis (0.5–2.0 GPa). The breaking of the nanoparticle starts when the W–C distances in the central part of the particle overcome 2.6 Å.

At the same Fig. 4, the plots for particles with vacancies are presented: (B) with a tungsten vacancy, (C) with a carbon vacancy, the both situated in the central plane of the particle. One can see that vacancies decrease the tensile strength, however, this influence is not drastic: the factor of decreasing is of about 0.7–0.8. Thus, defective nanoparticles keep well enough their durability in contrast with bulk material that can be broken easily if it has even a small crack.

4. Conclusions

Quantum–mechanical calculations show that at subnano level (1 nm or less) triangular particles compete with the particles having a cubic symmetry: the cubic particles are preferable if the number of atomic WC pairs (*N*) less than 15, but for $N > 15$ the triangular ones demonstrate the energy gain. The average W–C distances in trigonal particles stabilize quickly to the 2.04 Å, while in the cubic particles they have a tendency to growth up to the bulk value of 2.20 Å. Perhaps this is a main reason why the trigonal particles become more favorable at large particle sizes. Tensile strength for nanoparticles is predicted to be 10–15 times larger than the bulk value. Vacancies, either tungsten or carbon, decrease the tensile strength, however, this influence is not drastic: the factor of decreasing is of about 0.7–0.8. Thus, defective nanoparticles keep well enough their durability.

The electronic structure of WC nanoparticles looks like that of bulk *fcc*-WC with the position of the Fermi level near a local maximum of the DOS. One can suppose that the origin of such similarity is the similarity of W–C bonding in all our particles (either cubic or trigonal). This bonding is a NaCl-like, and the *fcc*-WC has the same bonding.

Acknowledgements

This work is supported by grants of the Russian Academy of Sciences and Russian Foundation for Basic Researches.

References

[1] Schubert WD, Bock A, Lux B. General aspects and limits of conventional ultrafine WC powder manufacture and hard metal production. Int J Refract Met Hard Mater 1995;13:281–6.
[2] Jia K, Fischer TE, Gallois B. Microstructure, hardness and toughness of nanostructure and conventional WC–Co composites. Nanostruct Mater 1998; 10:875–91.
[3] Kim BK, Ha GH, Lee DW, Lee GG, Ahn IS. Chemical processing of nanostructured cemented carbide. Adv Perform Mater 1998;5:341–52.
[4] Ferreira JAM, Pina Amaral MA, Antunes FV, Costa JDM. A study on the mechanical behavior of WC/Co hard metals. Int J Refract Met Hard Mater 2009;27:1–8.
[5] Christensen M, Wahnström G, Alibert C, Lay S. Quantitative analysis of WC grain shape in sintered WC–Co cemented carbides. Phys Rev Lett 2005;94:066105–9.
[6] Delanoe A, Lay S. Evolution of the WC grain shape in WC–Co alloys during sintering: effect of C content. Int J Refract Met Hard Mater 2009;27:140–8.
[7] Hohenberg H, Kohn W. Inhomogeneous electron gas. Phys Rev 1964;136: B864–71.

[8] Kohn W, Sham JL. Self-consistent equations including exchange and correlation effects. Phys Rev 1965;140:A1133–8.
[9] Cohen ML, Heine V. Pseudopotential theory of cohesion and structure. In: Ehrenreich H, Seitz F, Turnbull D, editors. Solid State Physics, vol. 24. New York: Academic Press; 1970. p. 38–249.
[10] Ceperley DM, Alder BJ. Ground state of the electron gas by a stochastic method. Phys Rev Lett 1980;45:566–9.
[11] Perdew JP, Zunger A. Self interaction correction to density functional approximations for many electron systems. Phys Rev B 1981;23:5048–79.
[12] Perdew JP, Wang Y. Accurate and simple density functional for the electronic exchange energy. Phys Rev B 1986;33:8800–2.
[13] Hamann DR. General norm-conserving pseudopotentials. Phys Rev B 1989;40:2980–7.
[14] Kleinman L, Bylander DM. Efficacious form for model pseudopotentials. Phys Rev Lett 1982;48:1425–8.
[15] Beckstedte M, Kley A, Neugebauer J, Scheffler M. Density functional theory calculations for poly-atomic systems: electronic structure, static and elastic properties and ab initio molecular dynamics. Comput Phys Commun 1997;107:187–205.
[16] Dabrowski J, Mussig H-J, Zavodinsky VG, Baierle R, Caldas MJ. Mechanism of dopant segregation to SiO_2/Si(0 0 1) intertfaces. Phys Rev B 2002;65:245–305.
[17] Zavodinsky VG. The mechanism of ionic conductivity in stabilized cubic zirconia. Phys Solid State 2004;46(3):453–7.
[18] Zavodinsky VG, Chibisov AN. Zirconia nanoparticles and nanostructured systems. J Phys: Conf Ser 2006;29:173–6.
[19] Zavodinsky VG, Chibisov AN. Influence of impurities on the stability and electronic states of titanium dioxide in the form of anatase. Phys Solid State 2009;51(3):507–13.
[20] Murnagham FD. The compressibility of media under extreme pressures. Proc Natl Acad Sci USA 1944;30:244–7.
[21] Fuchs M, Scheffler M. Ab initio pseudopotentials for electronic structure calculations of poly-atomic systems using density functional theory. Comput Phys Commun 1999;119:67–165.
[22] Troullier N, Martins JL. Efficient pseudopotentials for plane-wave calculations. Phys Rev B 1991;43:1993–2006.
[23] Monkhorst HJ, Pack JD. Special points for Brillouin-zone integrations. Phys Rev B 1976;13:5188–92.
[24] Site "Chemical encyclopedia/tungsten carbide". <http://www.xumuk.ru/encyklopedia/813.html>.
[25] Price DL, Cooper BP. Total energies and bonding for crystallographic structures in titanium–carbon and tungsten–carbon systems. Phys Rev B 1989;39:4945–77.
[26] Christensen M, Wahnström G. Co-phase penetration of WC(1 0 $\bar{1}$ $\bar{0}$)/WC(1 0 $\bar{1}$ $\bar{0}$) grain boundaries from first principles. Phys Rev B 2003;67:115415–25.
[27] Mattheiss LF, Hamman DR. Bulk and surface electronic structure of hexagonal WC. Phys Rev B 1984;30(4):1731–8.
[28] Liu AY, Wentzcovitch RM, Cohen ML. Structural and electronic properties of WC. Phys Rev B 1989;38:9483–9.
[29] Nabarro FRN, Bartolucci Luyckx S, Waghmare UV. Slip in tungsten monocarbide: I. Some experimental observations. Mater Sci Eng A 2008;483–484:139–42.
[30] Nabarro FRN, Bartolucci Luyckx S, Waghmare UV. Slip in tungsten monocarbide: II. A first-principles study. Mater Sci Eng A 2008;483–484:9–12.
[31] Kim C-S, Rohrer GS. Geometric and crystallographic characterization of WC surfaces and grain boundaries in WC–Co composites. Interface Sci 2004;12(1):19–27.
[32] Shatov AV, Firstov SA, Shatova IV. The shape of WC crystals in cemented carbides. Mater Sci Eng A 1998;242:7–14.
[33] Kim S, Han S-H, Park J-K, Kim H-E. Variation of WC grain shape with carbon content in the WC–Co alloys during liquid-phase sintering. Scripta Mater 2003;48(5):635–9.